Volume 34 | Number 10 | October 2019 | Pages 1945–2150

JAAS

Journal of Analytical Atomic Spectrometry

rsc.li/jaas

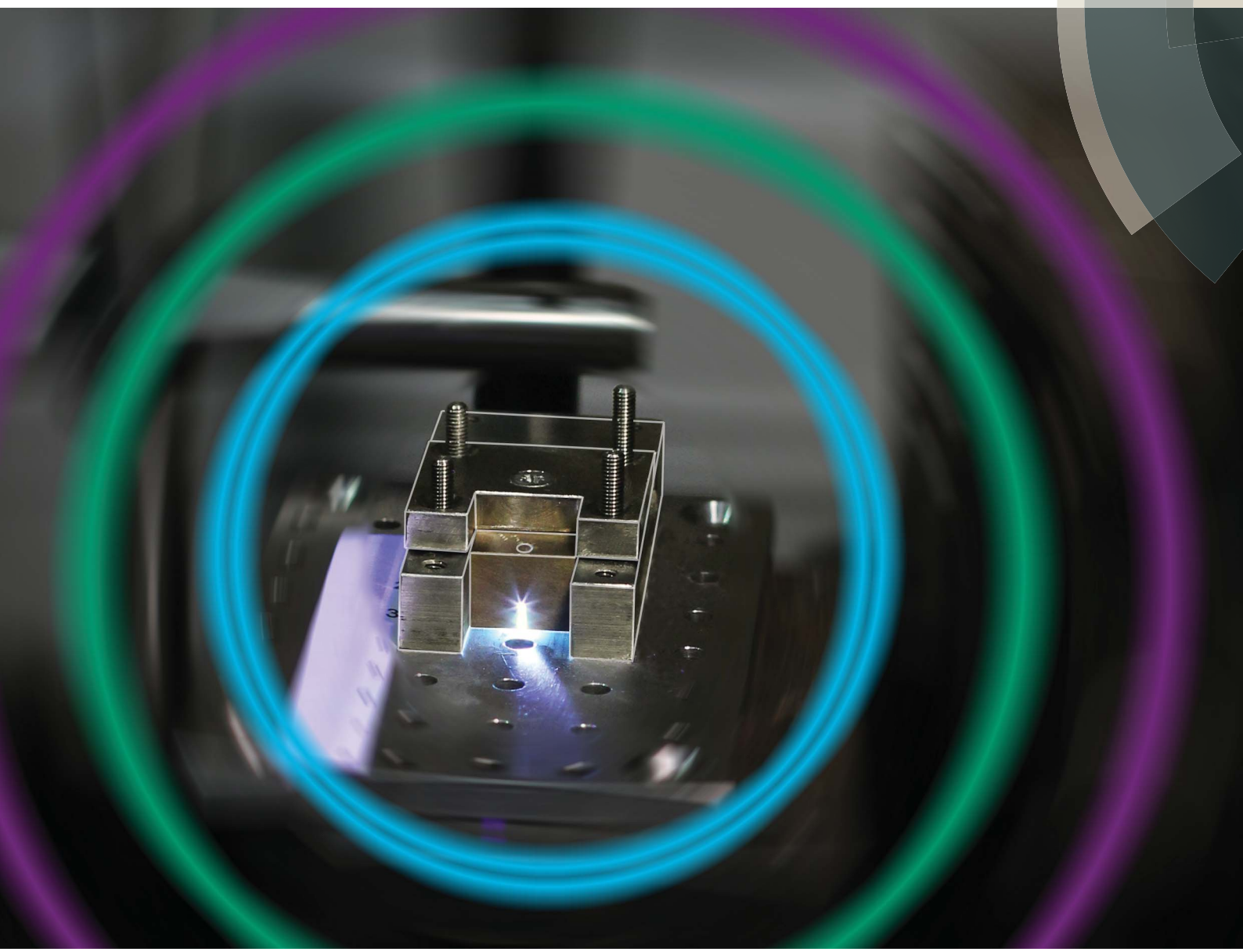

ISSN 0267-9477

ROYAL SOCIETY OF CHEMISTRY | Celebrating IYPT 2019

PAPER

Aleksandr S. Zakuskin, Andrey M. Popov and Timur A. Labutin

Shift of ionization equilibrium in spatially confined laser induced plasma

JAAS

PAPER

View Article Online
View Journal | View Issue

Cite this: *J. Anal. At. Spectrom.*, 2019, **34**, 1975

Shift of ionization equilibrium in spatially confined laser induced plasma

Aleksandr S. Zakuskin, Andrey M. Popov * and Timur A. Labutin

Spatial confinement of laser-induced plasmas has been recognized in the last decade as one of the ways to enhance the sensitivity of trace detection. However, there is no clear explanation for the fact that some lines are enhanced while others, in contrast, are weakened in confined plasma. In this work, we investigated the causes of the opposite changes of atomic and ionic lines in spatially confined plasma. For this purpose, we designed two cylindrical microchambers (2 and 4 mm in diameter) with side-on collection of emission. Plasma evolution in these chambers was studied at two laser energies: 70 mJ and 240 mJ. An accurate estimate of plasma parameters demonstrated that there were no changes in the low energy regime, while sharp changes both in T and especially Ne were observed for the two microchambers in the high energy regime. The features of evolution curves, such as the maximum and its temporal position, are explained by a shift of ionization equilibrium towards neutral atoms in the plasma after compression by the reflected shock wave. This clearly explains the differences in the evolution of the intensities of atomic and ionic lines: Al II 281.62 nm and Mg II lines are decreased rapidly, while atomic lines Sc I 402.37 nm and Mg I 277.98 nm are strongly enhanced at delays of 3–4 μs. Another observation is mixing of the plume and the consequent reduction of self-absorption for resonance lines due to collision of the shock wave with the plasma front.

Received 10th July 2019
Accepted 20th August 2019

DOI: 10.1039/c9ja00238c

rsc.li/jaas

Introduction

Laser-induced breakdown spectroscopy (LIBS) is a powerful analytical technique that can be used for the detection and characterization of materials. LIBS is a very simple spectroscopic technique, in which a focused laser beam is used to generate a plasma plume on the surface of solid and liquid samples or inside the volume of gases, liquids, and aerosols. LIBS has a distinct advantage over many other techniques. Since little or no sample preparation is needed before analysis, it can perform analyses on samples at a standoff distance and can be used for rapid real-time analysis in field operations.[1] However, LIBS gives way to the common techniques with sample dissolution in terms of sensitivity due to the small size of laser-induced plasma and its short lifetime. This fact constantly stimulates studies for sensitivity enhancement.[2,3]

Currently, several approaches are often utilized to increase the intensity of LIBS emission signals for the analysis of traces or hardly ionizable species: purging of an ablation cell with helium or argon gas, double-pulse excitation, resonant excitation of species in the plasma, additional excitation of laser ablation products by electric discharge or by microwaves, spatial confinement of the plasma in a microchamber (cavity), and the use of molecular emission. The most common approach is double-pulse LIBS, because, depending on the configuration, various parameters can be changed: evaporated mass, temperature and electron number density, and plasma volume and lifetime. Double-pulse orthogonal configuration with a pre-ablation spark in ambient gas can result in large signal enhancements (up to 10-fold increase of the signal-to-background ratio).[4] It is interesting to note that the enhancement factor of the emission signal for the orthogonal excitation scheme linearly depends on the excitation potential of the particular transition.[5] That is why this scheme is optimal for trace analysis,[6] although it significantly complicates the optical configuration and requires two lasers. The fluorescence measured simultaneously with the plasma emission[7–9] can enhance the sensitivity for one specific species, but it requires expensive tunable lasers. The increased plasma lifetime provided by an additional plasma source can also reduce the detection limits of trace element determination by LIBS. Electrical spark discharge induced after laser ablation[10–12] or microwave enhanced laser-induced plasma[13] results in long luminous for more than 1–10 ms. In the latter case, it is more accurate to consider the techniques like optical emission spectroscopy of microwave plasma or electric discharge with laser sampling. In summary it should be noted that all the considered methods of enhanced LIBS require complication of the LIBS instrument (the use of a specialized laser with two optical resonators or an additional laser, implementation of microwaves or a HV electrical generator).

Department of Chemistry, Lomonosov Moscow State University, 119234, Leninskie Gory, Moscow, Russia. E-mail: popov@laser.chem.msu.ru

In contrast, the use of molecular emission and spatial limitation of plasma expansion does not require redesign of the LIBS instrument.[14–17] Registration of molecular emission in laser-induced plasma allows the sensitive determination of fluorine, chlorine, bromine, and iodine in the form of their diatomic molecules with alkaline earth elements,[16,17] as well as isotopic analysis for several specific elements.[18] Thus, the spatial confinement of laser-induced plasma is the only universal approach for increasing sensitivity (up to 10-fold) without technical improvement of the instrument. The exceptional simplicity of the experiment with spatial confinement, which can be carried out even with a plate fixed at a few millimeters above the ablation spot, results in numerous applications for the analysis of coal,[19] soil,[15] steel,[20] and alloys,[21] and the plasma itself is limited by plates or chambers of cylindrical or spherical shape. This approach can also be implemented for femtosecond[22] and double-pulse[23,24] LIBS.

The enhancement of the LIBS signal is generally related to the effect of plasma confinement by the reflected shock wave generated during laser ablation,[25] whose propagation can significantly change the temperature and pressure profile of plasma.[26] At the same time, the available data on observed changes in plasma parameters differ significantly. Firstly, spatial confinement can not only increase, but also decrease the line intensity under optimal conditions, for example, Mg II 280.28 nm in soil, P I 255.32 nm/Cr I 433.08 nm in steel,[15] and C I 247.8 nm in graphite.[27] Only a few studies are devoted to the diagnostics of spatially confined laser-induced plasma, and in most cases open chambers or parallel plates (bilateral configuration) were used to confine the laser plume, and the results differ significantly between studies. Thus, in studies[14,21,28] a weak increase of temperature (900–1100 K) was observed for LIBS of aluminum and ore, while a significant increase of temperature (1500–3600 K) was found in ref. 20 and 29. In the latter case, it seems that the temperature was overestimated, since intense lines of the main components were involved in calculations. Unfortunately, numerical simulation of evolution of plasma temperature was performed only for extreme conditions: up to 3 ns (ref. 30) or for a giant energy pulse of 100 J.[31] In view of the significant influence of cavity configuration on the degree of plasma compression, an increase in the intensity of the Cu plasma and its temperature for various cavity configurations was thoroughly considered in ref. 32. The strongest growth of the emission intensity (4 times) and temperature (up to 1500 K) was observed from the round cavity due to effective plasma confinement, while the bilateral configuration provided a weak amplification (1.5 times) at almost the same temperature. Obviously, the limitation restriction of plasma expansion should influence the spatial profile of the laser plume. The shadowgraph images demonstrated that the shockwave reflection from the cavity wall resulted in a more compact plasma and a better position stability of the plasma core.[33] Spatial and temporal resolution measurements of plasma expansion in an open chamber (1 mm height) clearly demonstrated that the plasma was displaced through the open side of the cavity and, therefore, the spatial and temporal emission was not significantly influenced by its height if the cavity was higher than the vapor plume.[34] At the same time, the evaluation of the temperature seems to be inadequate, because the lines used for plasma diagnostics undoubtedly were strongly self-absorbed (the theoretical ratio of copper lines in the multiplet $^2D–^2P^\circ$ is 0.53 (ref. 35) and the observed one was close to 0.75). Therefore, in the current study, we aimed at an accurate evaluation of the plasma temperature and electron number density to study the evolution of spatially confined plasma. We also considered the relationship of plasma parameters with the intensity of emission lines. We studied both ionic and atomic lines (both resonant and non-resonant) in order to reveal the particular changes in laser-induced plasma caused by the propagation of the shock wave.

Experimental

Experimental set-up

We used a typical experimental LIBS set-up described in detail in our work[36] slightly modified with microchamber mounting. The second harmonic of a Q-switched Nd:YAG laser (model LS-2134UTF, LOTIS TII, Belarus) with a pulse duration of ≈6 ns and a beam diameter of ≈6 mm was used. We designed and manufactured special cylindrical microchambers for conducting LIBS experiments with spatially confined plasma (Fig. 1). The internal diameter is equal to the height and it is 2 and 4 mm for the used microchambers. The microchamber was placed on a sample holder and its bottom surface was in a tight contact with the surface of a target. An aluminum–copper–lithium alloy

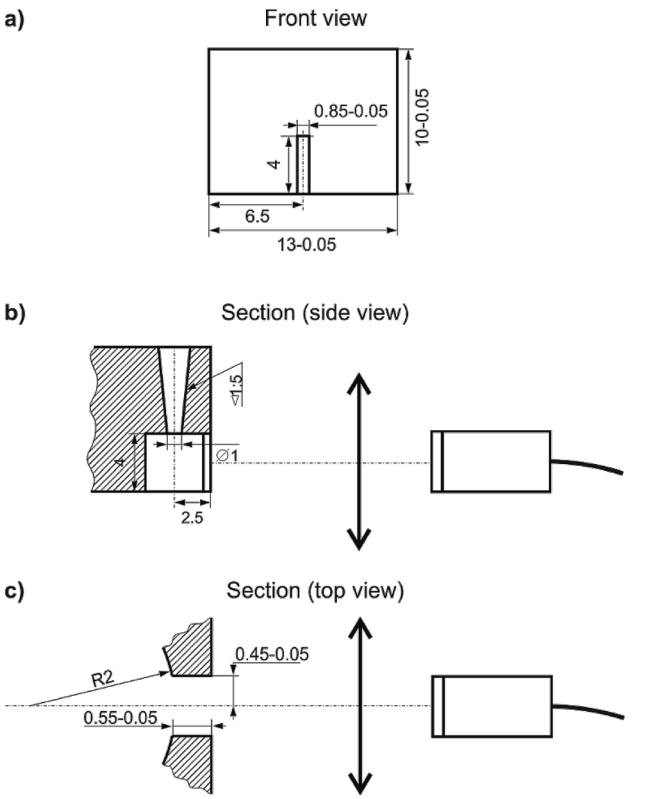

Fig. 1 Scheme of the 4 mm microchamber and emission collection system in the front view (a), side view (b) and top view (c). $R2 = 2$ mm.

containing 2.9 ± 0.2 wt% Cu, 1.06 ± 0.05 wt% Li, and 0.59 ± 0.01 wt% Mg served as a target. Laser radiation passed through the small vertical conical hole (1 mm in diameter and tapering index of 1 : 5) and focused 8 mm below the sample surface, resulting in a spot with a diameter of ≈400 μm. Plasma radiation was collected *via* a slit cut along the front side of the chamber. The slit has the same height as the chamber (2 or 4 mm) and a width of 0.5 mm and 0.85 mm for 2 mm and 4 mm chambers, respectively. The radiation was projected to the end of a line-to-line optical fiber by a spherical lens with a 2-fold decrease. Another end of the fiber directed radiation onto the 30 μm slit of a Czerny-Turner spectrometer (HR-320, ISA, USA) that provides a resolution of ≈10 000 at 280 nm and ≈21 500 at 400 nm with a grating of 3600 lines per mm. Plasma emission spectra were recorded by using an ICCD camera (Nanogeit-2V, NANOSCAN, Russia) with the use of laboratory-made software.[36] Measurements were carried out for two pulse energies: 70 mJ and 240 mJ (laser fluence ≈ 56 J cm^{-2} and ≈190 J cm^{-2}). Spectra were recorded for freely expanding and spatially confined plasma at delays from 0.5 μs to 10 μs. The gate width was 100 ns for spectra in the range near 280 nm and 500 ns in the range near 400 nm to maintain a high ratio of delay to gate as it is recommended by Aragon and Aguilera for plasma diagnostics.[37] To keep the signal-to-noise ratio (SNR) above 25 we accumulated up to 20 laser pulses. Each final spectrum is the average of at least 25 recorded spectra. Typical spectra of the two ranges containing all the considered lines are shown in Fig. 2. All lines were fitted by the Lorentz function, taking into account an instrumental width at 280 nm of 26.3 ± 0.7 pm as estimated in our previous work.[38]

Plasma diagnostics

We calculated the plasma temperature using the lines of Mn a^{6}S–z^{6}P° and a^{6}D–z^{6}D multiplets (see Table 1) assuming the existence of Local Thermodynamic Equilibrium (LTE).[37] Temperature T and its uncertainty ΔT were obtained from the Boltzmann plot constructed for these multiplets. Due to spectral interference at early delays (up to 3000 ns), the intensity of Mn I 403.07 nm becomes overestimated, so it was excluded from temperature determination for those points where the intensity ratios of Mn I 403.07/Mn I 403.31 and Mn I 403.07/Mn I 403.31 were far from theoretically predicted values.

The electron number density (N_e) of plasma was estimated by Stark broadening of the Al II 281.62 nm emission line. We neglected the self-absorption of the line due to high energy (7.42 eV,[35] see Table 1) of its lower level. The electron impact half–half width is 21.2 pm (ref. 39) for an electron number density of 10^{16} cm^{-3} at 10 500 K (accuracy of 10%). Since Doppler broadening calculated by using the equation[40]

$$\omega_d = 0.5 \times 7.16 \times 10^{-7} \lambda \sqrt{\frac{T}{M}},$$

where λ is the wavelength (Å), T is the plasma temperature (K) and M is the atomic weight (a.u.m), was sufficiently lower (3 pm) than the measured HWHM of the line (30–500 pm) we neglected Doppler broadening.

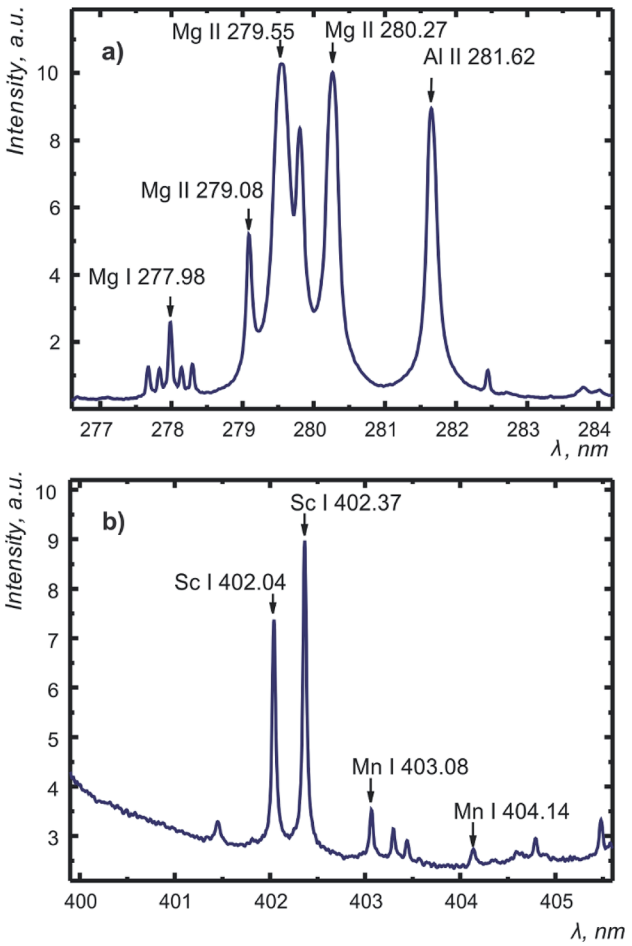

Fig. 2 Emission spectra of laser-induced plasma obtained for an Al alloy sample within two spectral ranges: 280 nm (a) and 403 nm (b). Delay and gate were 2.5 μs and 100 ns, respectively.

Results and discussion

Plasma parameters

The temporal evolution of temperature and electron number density is shown in Fig. 3. We estimated these parameters for plasma evolution from 0.5 μs to 8 μs. As one can see, a higher temperature was obtained in the case of higher laser pulse energy for freely expanding plasma. At short delays (up to 3–4 μs), the difference between spatially confined and freely expanding plasmas is negligible within the uncertainty for both pulse energies. It should be emphasized that we did not observe any significant deviations in temperature curves such as local maxima or inflection points. The differences in the evolution of excitation temperature for freely expanding plasma can be related to the energy deposited by the laser plume during ablation. It was shown that the dynamics of plasma expansion and contraction due to cooling *via* the ambient air is related to the pulse energy. Therefore, the temperature of the laser plasma was relatively stable after the end of expansion and before the start of rapid contraction.[42] In contrast, some significant peculiarities were observed in the curves demonstrating the evolution of electron number density (Fig. 3). For low pulse energy (70

Table 1 Parameters of transitions for Mn I and Al II lines used for plasma diagnostics

#	Species	Configuration and term	Wavelength, nm	g_kA_{ki}, 10^7 s^{-1}	$\Delta A/A$, %	E_{lower}, eV	E_{upper}, eV
1	Mn I	$3d^54s^2$–$3d^5(^6S)4s4p(^3P^\circ)$ a^6S–z^6P	403.08 (ref. 41)	13.9 (ref. 41)	3	0.000	3.075
2	Mn I		403.31	9.9 (ref. 41)	18	0.000	3.073
3	Mn I		403.45	6.32 (ref. 41)	18	0.000	3.072
4	Mn I	$3d^6(^5D)4s$–$3d^6(^5D)4p$ a^6D–z^6D	404.14 (ref. 41)	78.7 (ref. 41)	3	2.114	5.181
5	Al II	$3s3p$–$3s4s$ $^1P^\circ$–^1S	281.62	35.7	3	7.421	11.822

mJ per pulse, see Fig. 3c), N_e decreases monotonically in all 3 cases of freely expanding and confined plasmas. Although the N_e of freely expanding plasma in the case of higher laser pulse energy (240 mJ per pulse, see Fig. 3d) demonstrates the same trend, the curves corresponding to both microchambers have pronounced peculiarities. It is important to note that they occur at different times: we observe a distinct curvature at around 1 μs for the 2 mm chamber and a local maximum at 2.5 μs for the 4 mm one. These specific times are likely to be related to the size of the microchamber and to the time needed for the shock wave propagation to the microchamber wall, reflection and return paths to the collision with the plasma front. According to the estimation[43] of the velocity of shock waves in air ($\approx 4 \times 10^3$ m s^{-1}), it takes ≈ 1 and ≈ 2 μs to pass from the center of the chamber to the wall and back in 2 mm and 4 mm chambers, respectively.

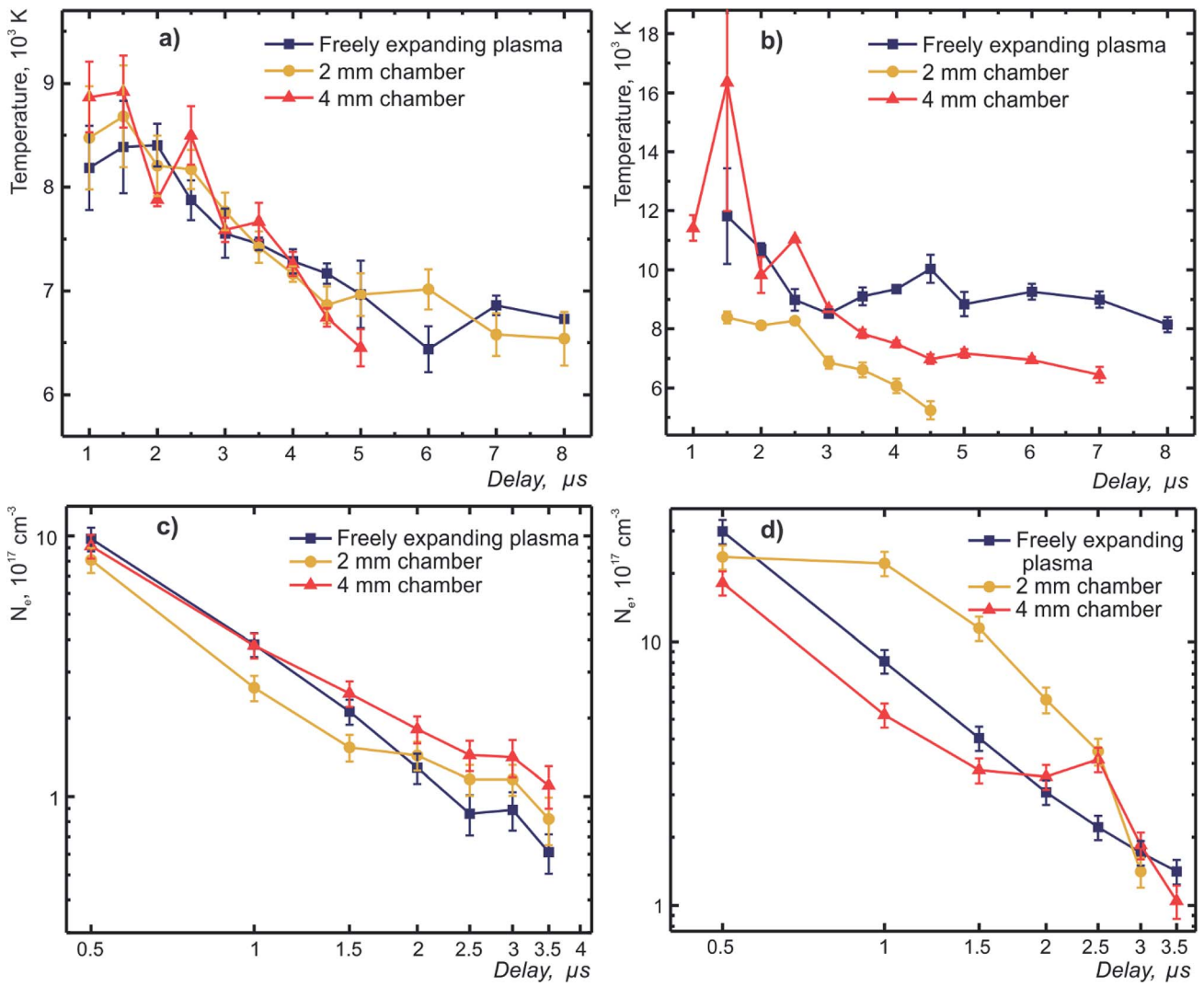

Fig. 3 Temperature (top) and electron density (bottom) as a function of delay for freely expanding plasma and spatially confined plasma in microchambers for two pulse energies: 70 mJ (a and c) and 240 mJ (b and d). Diameters of the chambers are indicated in a legend.

Intensity of lines

Additional details of the shock wave's influence on laser-induced plasma can be retrieved from the temporal evolution of lines' intensities. As one can see in Fig. 4, the intensity of the aluminium ionic line Al II 281.62 nm significantly differs for confined and freely expanding plasma. In the case of higher pulse energy (Fig. 4b), a sharp decline in the intensity was observed from a delay of 1.5 and 2.5 μs for 2 mm and 4 mm chambers, respectively. As in the case of plasma parameters, lower pulse energy leads to a monotonic decrease in the line intensity without significant features. It is important to note that the considered line is an ionic one with a high energy of the upper level of transition (11.8 eV).

In contrast, a fundamentally different temporal evolution of intensity was observed for a resonant atomic scandium line Sc I 402.04 nm as it is shown in Fig. 4c and d. With any microchamber and any pulse energy the line intensity exceeds the corresponding value without spatial confinement. Maximal enhancement (intensity increased 6.5 times) was achieved in the 4 mm chamber with high pulse energy (Fig. 4d). In the case of a pulse energy of 70 mJ, both curves demonstrate maximum at the same delay of ≈2.5 μs (Fig. 4c). However, the evolution of signal intensity differed significantly for the 4 mm chamber. The maximum of intensity is at 4 μs delay, approximately 1.5 μs later than the local maximum observed for plasma electron number density, and although the curve for the 2 mm chamber has the same pattern, the maximum is only 1 μs later than the break in N_e evolution. These observations, combined with the data of plasma diagnostics, demonstrate that after the collision of the reflected shock wave with the plasma front, N_e stops falling or even increases slightly. Simultaneously, the intensity of atomic lines rises significantly over a period of time, while the ion emission drops sharply to zero. Plasma confinement by the back-reflected shock wave leads to a short-term termination of the plasma expansion which in turn causes the observed stop of N_e decrease (see Fig. 3d). Therefore, the ionization equilibrium is shifted towards neutral atoms leading to the described changes in the intensities of ionic and atomic lines.

Since all the above effects are most pronounced for a laser pulse energy of 240 mJ in the 4 mm microchamber, we made further investigations of magnesium lines only for this combination of experimental parameters. Firstly, Fig. 5 shows the time dependence of the ratio of lines' intensities in confined and freely expanding plasma (the so-called enhancement

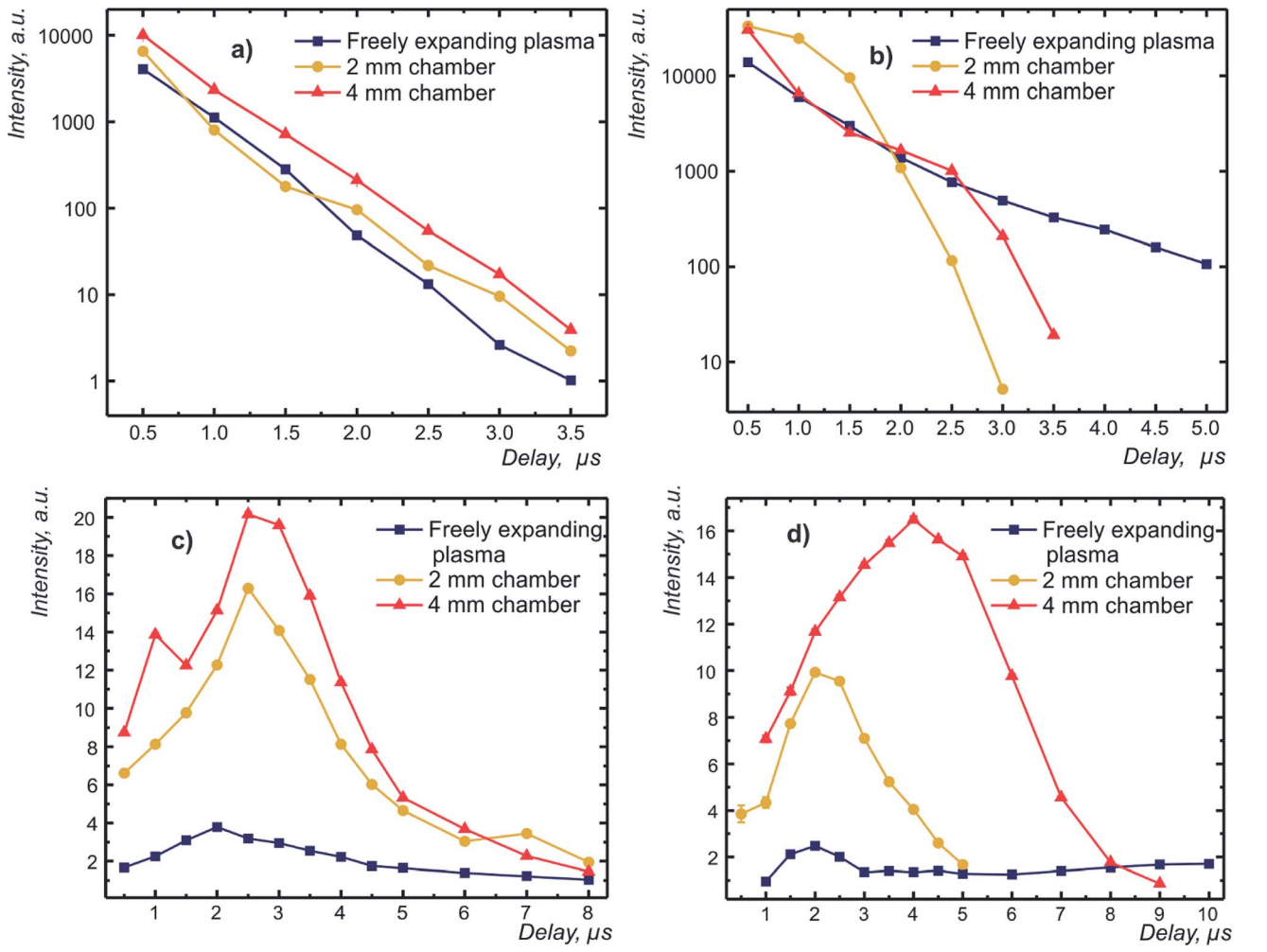

Fig. 4 Intensity of Al II 281.62 nm (top) and Sc I 402.37 nm (bottom) as a function of delay for freely expanding plasma and spatially confined plasma in microchambers for two pulse energies: 70 mJ (a and c) and 240 mJ (b and d). Diameters of the chambers are indicated in a legend.

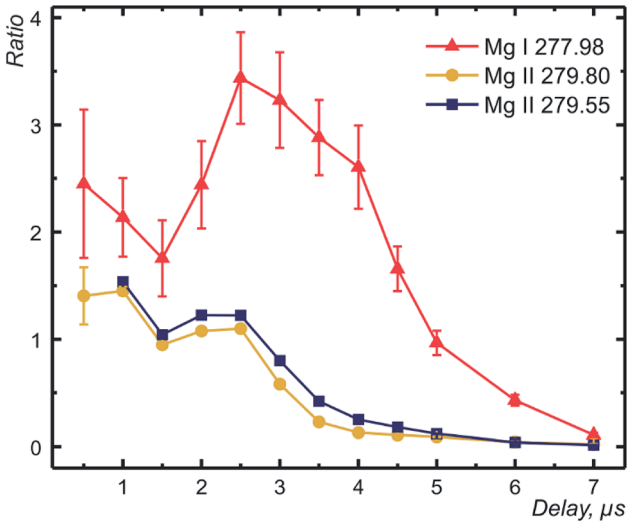

Fig. 5 Intensity ratio of atomic Mg I 277.98 nm, ionic non-resonant Mg II 279.80 nm and ionic resonant Mg II 279.55 nm lines in spatially confined (4 mm chamber) to freely expanding plasma as a function of delay.

factor). Up to 2.5 μs, the ratio for ionic lines (resonant Mg II 279.55 nm and non-resonant Mg II 279.80 nm) is slightly above 1 and drops sharply after 2.5 μs. At the same time, the curve for the atomic Mg I 279.98 nm line clearly demonstrates the maximal signal enhancement by 3.4 times at a delay of 2.5 μs. Thus, the use of microchambers allows one to significantly increase the intensity of atomic lines while almost not affecting the intensity of ionic lines at early delays.

Besides the influence of the shock wave on plasma density, the distribution of ions and atoms, excited and ground state particles, should change inside the plume. To reveal the particular changes, we compared the intensity ratios of lines

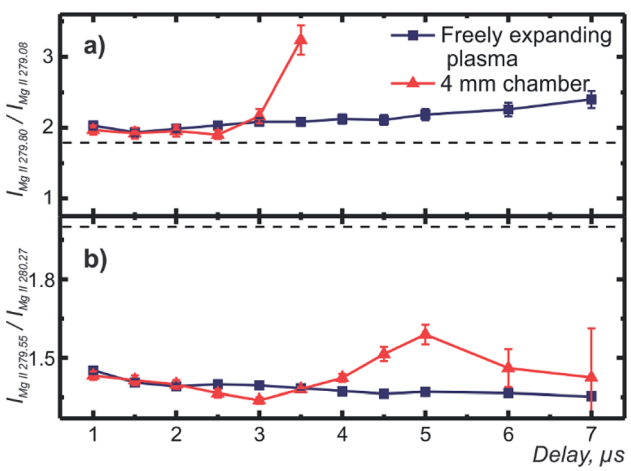

Fig. 6 Ratio of intensities of the non-resonant doublet Mg II 279.80 nm/Mg II 279.08 nm (a) and the resonant doublet Mg II 279.55 nm/Mg II 280.27 nm (b) in freely expanding and spatially confined (4 mm chamber) plasma as a function of delay with a pulse energy of 240 mJ. Dashed lines show the theoretical values of ratios for these pairs of emission lines.

within the same multiplet. As one can see in Fig. 6b, the ratio of resonant lines ($I_{\text{Mg II 279.55}}/I_{\text{Mg II 280.27}}$) is far from the theoretical value (2) for both the freely expanding plasma or the confined one because of the self-absorption effect. After backward shockwave propagation the ratio increased to ≈1.6 at 3 μs. Apparently, the noticeable reduction of self-absorption is related to plasma homogenization by the shock wave. Another tendency was observed for the ratio of non-resonant lines ($I_{\text{Mg II 279.80}}/I_{\text{Mg II 279.08}}$, see Fig. 6a). It is much closer to the theoretical value (1.8) because of the lower intensity of lines and, therefore, the lower influence of self-absorption. Moreover, the ratio starts increasing rapidly from 2.5 μs and reaches a value of ≈3.2 in the case of plasma confinement in the microchamber. It can be explained by the simultaneous rapid decrease of the intensity of magnesium ionic lines and increase of the intensity of the atomic Mn I 279.83 nm line that is completely overlapped with Mg II 279.80 nm and makes a significant contribution to the measured intensity. Both of these effects are in good agreement with the conclusions made above for Al and Sc lines.

Conclusions

To investigate why some emission lines increase but others decrease in spatially confined plasma, the evolution of plasma temperature and its electron density was examined for two specially designed chambers with a diameter of 2 mm and 4 mm. The temporal behavior of plasma parameters strongly depended on the laser energy used. In contrast to many previous studies no evident change of temperature or electron density was observed at 70 mJ per pulse (≈56 J cm^{-2}) for both chambers. At the same time, an increase of energy up to 240 mJ per pulse (≈190 J cm^{-2}) resulted in a moderate decrease of T for confined plasma and significant changes in electron density. Since the density changed, the intensity of ionic lines (both Al II and Mg II) decreased significantly at the time of possible shock wave collision with the plasma front. Resonance atomic lines (Sc I) had another behaviour: their intensities increased by several times. We suggest that recombination leads to formation of atoms in highly excited states which are collisionally decayed to the states to be dipole-coupled to the ground state. Such a suggestion is confirmed by the fact that atomic lines reached their maximum intensity much later than the possible collision of the reflected shock wave with the plasma front. The collision of the shock wave with the plasma front shifts ionization equilibrium towards neutral atoms, which confirms the temporal behaviour of atomic lines. Actually, an increase in Ne leads to a shift in the equilibrium M+ + Ne ↔ M. Another possible competing process is ionization due to the presence of an easily ionizable element, *i.e.* M+ + N ↔ M + N+, where the ionization potential of M is larger than that of N. Since aluminium has a lower ionization potential (5.98 eV), the ionization of scandium (6.56 eV) and magnesium (7.64 eV) will be suppressed. Therefore, atomic lines will be amplified in the same way as after the addition of ionization buffer.[44] Assumed mixing of the plasma plume can result in homogenization of the plasma composition. We observed that the self-absorption effect for resonance magnesium lines was reduced with the use of both microchambers. Summarizing our

observation, the enhancement effect of microchambers is fruitful to determine elements with the use of resonant atomic lines. Since such lines are usually self-absorbed, spatial confinement can diminish the effect. Moreover, this mechanism allows reasonable interpretation of the observed growth of the line intensity of the main component (copper lines in pure copper,[45] carbon in coal,[29] and aluminium in aluminium-base alloy[14]).

Conflicts of interest

There are no conflicts to declare.

References

1 D. M. Wong, A. A. Bol'shakov and R. E. Russo, in *Encyclopedia of Spectroscopy and Spectrometry*, 2017, pp. 533–538, DOI: 10.1016/b978-0-12-803224-4.00062-5.
2 Y. Li, D. Tian, Y. Ding, G. Yang, K. Liu, C. Wang and X. Han, *Appl. Spectrosc. Rev.*, 2017, **53**, 1–35.
3 N. B. Zorov, A. M. Popov, S. M. Zaytsev and T. A. Labutin, *Russ. Chem. Rev.*, 2015, **84**, 1021–1050.
4 D. N. Stratis, K. L. Eland and S. M. Angel, *Appl. Spectrosc.*, 2000, **54**, 1270–1274.
5 C. Gautier, P. Fichet, D. Menut, J.-L. Lacour, D. L'Hermite and J. Dubessy, *Spectrochim. Acta, Part B*, 2004, **59**, 975–986.
6 E. Tognoni and G. Cristoforetti, *J. Anal. At. Spectrom.*, 2014, **29**, 1318–1338.
7 W. Sdorra, A. Quentmeier and K. Niemax, *Mikrochim. Acta*, 1989, **98**, 201–218.
8 X. K. Shen, H. Wang, Z. Q. Xie, Y. Gao, H. Ling and Y. F. Lu, *Appl. Opt.*, 2009, **48**, 2551–2558.
9 C. M. Li, Z. Q. Hao, Z. M. Zou, R. Zhou, J. M. Li, L. B. Guo, X. Y. Li, Y. F. Lu and X. Y. Zeng, *Opt. Express*, 2016, **24**, 7850–7857.
10 L. Moenke-Blankenburg, *Laser Microanalysis*, Wiley, New York, 1989.
11 M. V. Belkov, V. S. Burakov, A. De Giacomo, V. V. Kiris, S. N. Raikov and N. V. Tarasenko, *Spectrochim. Acta, Part B*, 2009, **64**, 899–904.
12 S. Eschlböck-Fuchs, P. J. Kolmhofer, M. A. Bodea, J. G. Hechenberger, N. Huber, R. Rössler and J. D. Pedarnig, *Spectrochim. Acta, Part B*, 2015, **109**, 31–38.
13 M. Tampo, M. Miyabe, K. Akaoka, M. Oba, H. Ohba, Y. Maruyama and I. Wakaida, *J. Anal. At. Spectrom.*, 2014, **29**, 886–892.
14 X. K. Shen, J. Sun, H. Ling and Y. F. Lu, *J. Appl. Phys.*, 2007, **102**, 093301.
15 A. M. Popov, F. Colao and R. Fantoni, *J. Anal. At. Spectrom.*, 2010, **25**, 837–848.
16 M. Gaft, L. Nagli, N. Eliezer, Y. Groisman and O. Forni, *Spectrochim. Acta, Part B*, 2014, **98**, 39–47.
17 M. Gaft, L. Nagli, Y. Raichlin, F. Pelascini, G. Panzer and V. M. Ros, *Spectrochim. Acta, Part B*, 2019, **157**, 47–52.
18 A. A. Bol'shakov, X. Mao, J. J. González and R. E. Russo, *J. Anal. At. Spectrom.*, 2016, **31**, 119–134.
19 Z. Y. Hou, Z. Wang, J. M. Liu, W. D. Ni and Z. Li, *Opt. Express*, 2013, **21**, 15974–15979.
20 L. B. Guo, C. M. Li, W. Hu, Y. S. Zhou, B. Y. Zhang, Z. X. Cai, X. Y. Zeng and Y. F. Lu, *Appl. Phys. Lett.*, 2011, **98**, 131501.
21 C. M. Li, L. B. Guo, X. N. He, Z. Q. Hao, X. Y. Li, M. Shen, X. Y. Zeng and Y. F. Lu, *J. Anal. At. Spectrom.*, 2014, **29**, 638–643.
22 X. Wang, A. Chen, Y. Wang, D. Zhang, L. Sui, D. Ke, S. Li, Y. Jiang and M. Jin, *Phys. Plasmas*, 2017, **24**, 103305.
23 X. Su, W. Zhou and H. Qian, *J. Anal. At. Spectrom.*, 2014, **29**, 2356–2361.
24 L. B. Guo, B. Y. Zhang, X. N. He, C. M. Li, Y. S. Zhou, T. Wu, J. B. Park, X. Y. Zeng and Y. F. Lu, *Opt. Express*, 2012, **20**, 1436–1443.
25 B. Campanella, S. Legnaioli, S. Pagnotta, F. Poggialini and V. Palleschi, *Atoms*, 2019, **7**, 57.
26 R. Kodama, K. A. Tanaka, M. Nakai, K. Nishihara, T. Norimatsu, T. Yamanaka and S. Nakai, *Phys. Fluids B*, 1991, **3**, 735–744.
27 F. L. Huang, P. P. Liang, X. Yang, H. Cai, J. D. Wu, N. Xu, Z. F. Ying and J. Sun, *Phys. Plasmas*, 2015, **22**, 063509.
28 A. S. Zakuskin, A. M. Popov, N. B. Zorov and T. A. Labutin, *Tech. Phys. Lett.*, 2018, **44**, 73–76.
29 Z. Wang, Z. Y. Hou, S. L. Lui, D. Jiang, J. M. Liu and Z. Li, *Opt. Express*, 2012, **20**, A1011–A1018.
30 C. Li, J. Wang and X. Wang, *Phys. Lett. A*, 2014, **378**, 3319–3325.
31 D. P. Singh, M. A. Harith, V. Palleschi, M. Vaselli and E. Panarella, *J. Fusion Energy*, 1990, **9**, 513–516.
32 Q. Y. Wang, A. M. Chen, D. Zhang, Y. Wang, L. Z. Sui, S. Y. Li, Y. F. Jiang and M. X. Jin, *Phys. Plasmas*, 2018, **25**, 073301.
33 Y. T. Fu, Z. Y. Hou and Z. Wang, *Opt. Express*, 2016, **24**, 3055–3066.
34 X. Li, Z. Wang, X. Mao and R. E. Russo, *J. Anal. At. Spectrom.*, 2014, **29**, 2127–2135.
35 A. Kramida, Yu. Ralchenko, J. Reader and NIST ASD Team, *NIST Atomic Spectra Database*, 2019, https://physics.nist.gov/asd, DOI: 10.18434/T4W30F.
36 S. M. Zaytsev, A. M. Popov, N. B. Zorov and T. A. Labutin, *J. Instrum.*, 2014, **9**.
37 C. Aragon and J. A. Aguilera, *Spectrochim. Acta, Part B*, 2008, **63**, 893–916.
38 A. M. Popov, T. F. Akhmetzhanov, T. A. Labutin, S. M. Zaytsev, N. B. Zorov and N. V. Chekalin, *Spectrochim. Acta, Part B*, 2016, **125**, 43–51.
39 C. Colon, G. Hatem, E. Verdugo, P. Ruiz and J. Campos, *J. Appl. Phys.*, 1993, **73**, 4752–4758.
40 N. Konjevic, *Phys. Rep.*, 1999, **316**, 339–401.
41 A. J. Booth, D. E. Blackwell, A. D. Petford and M. J. Shallis, *Mon. Not. R. Astron. Soc.*, 1984, **208**, 147–159.
42 N. Kawahara, J. L. Beduneau, T. Nakayama, E. Tomita and Y. Ikeda, *Appl. Phys. B: Lasers Opt.*, 2007, **86**, 605–614.
43 A. M. Popov, F. Colao and R. Fantoni, *J. Anal. At. Spectrom.*, 2009, **24**, 602–604.
44 A. M. Popov, A. N. Drozdova, S. M. Zaytsev, D. I. Biryukova, N. B. Zorov and T. A. Labutin, *J. Anal. At. Spectrom.*, 2016, **31**, 1123–1130.
45 X. Gao, L. Liu, C. Song and J. Lin, *J. Phys. D: Appl. Phys.*, 2015, **48**, 175205.